PRELIMINARY FARADAY ROTATION RESULTS ASSOCIATED WITH THE PHOTOIONIZED GAS OF IC 1396

Ramisa Akther Rahman[1] and Allison H. Costa[2]

[1]William & Mary, 200 Stadium Drive, Williamsburg, VA 23185, USA

[2]National Radio Astronomy Observatory, 520 Edgemont Road, Charlottesville, VA 22903, USA

Abstract

We present initial Faraday rotation measurements of extragalactic radio sources with lines of sight passing through or near to the HII region of IC 1396. We measured the linear polarization of the sources with the Karl G. Jansky Very Large Array (VLA) at frequencies of $\sim$5 GHz (6 cm). We estimate the background Rotation Measure (RM) in this region of the galaxy to be ~ -140 rad m^{-2}. We find the sources having lines of sight passing through IC 1396 have an excess $|\mathrm{RM}|$ of $\sim$ 62–465 rad m^{-2} with respect to the background. We discuss the RM values in the context of magnetized plasma of IC 1396. We also discuss a simple shell model to reproduce $|\mathrm{RM}|$ as a function of the distance from the center of IC 1396. We additionally present electron density results from this modeling of the structure of IC 1396.

1. Introduction

Stars form within molecular clouds that are comprised of cold ($\sim$10 K) gas and dust. Massive stars, such as O and B type stars, impact these clouds by emitting photons at 13.6 eV. These photons ionize neutral hydrogen gas, forming a sphere-like region of HII gas around the star (Strömgren, 1939).

These HII regions are hot plasmas containing free electrons and can reach temperatures of 10,000 K. Particles within plasma tend to follow magnetic field lines. Hence, magnetic fields within HII regions can greatly influence the dynamics and the evolution of HII regions, supporting molecular clouds against future collapse (quenching star formation) or potentially triggering star formation.

The HII region of interest, IC 1396 lies in the plane of the Milk Way galaxy, which has its own magnetic field that is thought to follow the spiral arms of the galaxy (Van Eck et al., 2011). In this work, we investigate the polarity and the magnitude of the magnetic field near IC 1396 to understand how the galactic magnetic field is modified within the H II region.

1.1. Faraday Rotation as a Technique for Assessing Magnetic Fields

A technique of assessing the polarity and magnitude of magnetic fields is Faraday rotation. This is the rotation of the polarization plane of a radio wave as it travels through magnetized plasma, such as an HII region. The polarization position angle χ of a source is given by:

$$\chi = \chi_0 + \left[\left(\frac{e^3}{2\pi m_e^2 c^4} \right) \int_0^L n_e \vec{B} \cdot \vec{ds} \right] \lambda^2 \qquad (1)$$

where χ is the polarization position angle, χ_0 is intrinsic polarization position angle, e is the fundamental electric charge, m_e is the mass of an electron, c is the speed of light, λ is the wavelength, n_e is the electron density, $\vec{B}$ is the magnetic field, and $\vec{ds}$ is the incremental pathlength interval along the line of sight. The integral is taken from the source $s = 0$ to the observer at $s = L$, with the integral over the dot product resulting in the parallel component of the magnetic field. As areas except the HII region are assumed to have no electron density n_e, L becomes the effective thickness of the HII region. The Rotation Measure (RM) is defined as the quantities in the square brackets in Equation 1. Figure 1 is an illustration of an electromagnetic wave propagating through plasma with a magnetic field.

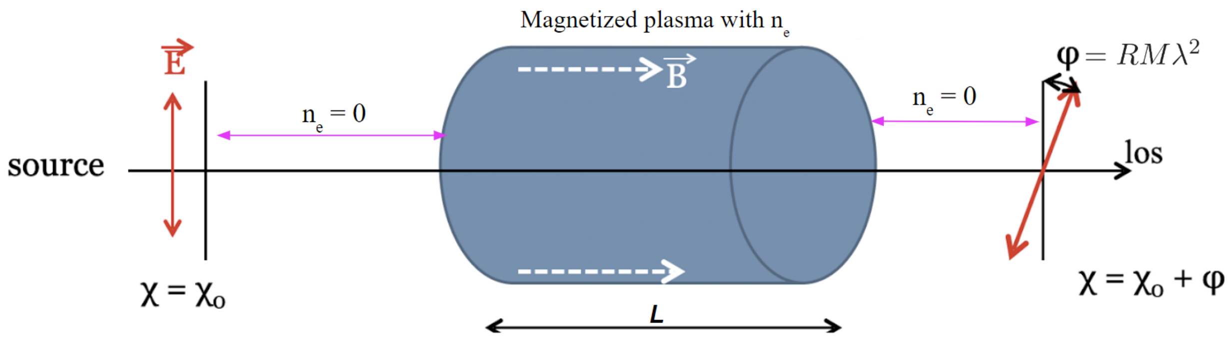

Figure 1: This illustration depicts the propagation of a radio wave emitted from a source. The line of sight passes through the magnetized plasma and reaches an antenna, with the magnetic field of the region causing the wave to rotate by an angle φ. This phenomenon is Faraday rotation. The quantities of n_e, $\vec{B}$, L, χ_0 are defined in the text.

The radio sources act as a probe of the HII. we assessed the polarimetric properties of extragalactic radio sources with lines of sight through or near the HII region. These galaxies emit a type of non-thermal radiation known as synchrotron. This is linearly polarized light and is emitted when relativistic electrons accelerate in a spiral path along the strong magnetic fields of these galaxies. Photons in HII regions do not typically emit linearly polarized light, so it is reasonable to assume the linearly polarized signals we detect are due to the selected sources. Though the HII region does not emit linearly polarized light, it is a plasma, so the electromagnetic fields within the plasma will alter the linearly polarized light that is propagating through the plasma. Hence, any change in the polarization position angle χ of the radiation from the extragalactic sources should be in response to the magnetic field of the HII region.

The RM value contains the magnetic field and electron density information. we calculate the RM value by plotting χ data versus λ^2 and obtaining the slope, where λ^2 is coming from the range of frequencies observed. This relationship is shown in Equation (2).

$$\mathrm{RM} = \frac{\Delta\chi}{\Delta(\lambda^2)} \tag{2}$$

1.2. IC 1396 as a Region of Interest

IC 1396, known as the Elephant Trunk's Nebulae, is an HII region in the Cepheus constellation. It is ionized by the triplet star cluster HD 206267A. One of the stars responsible for ionization is a young massive star of an O spectral type. (Chlebowski and Garmany, 1991). Figure 2 shows a image of IC 1396 with the position of all the extragalactic sources. The distance to IC 1396 is 918 pc and it has an angular size of 35.6', with R.A.(J2000) = $21^{\mathrm{h}}\ 37^{\mathrm{m}}\ 25.6^{\mathrm{s}}$, decl.(J2000) = $57^\circ\ 17'\ 14''$ (Tarricq et al., 2021). We chose to study IC 1396 with the Faraday Rotation technique as it meets the criteria used to select both the Rosette Nebula and W4 of being in the galactic anticenter direction, known distance and mass loss rate, (Costa and Spangler, 2018; Costa et al., 2016). Furthermore, there are not as many HII regions along the lines of sight that would interfere with measurements, which is important for our assumption that areas external to IC 1396 (along the line of sight) have no electron density.

2. Observations

The data used in this research were observed in 2014 with the Karl G. Jansky Very Large Array (VLA). The data consist of 31 extragalactic sources with lines of sight passing through or near to IC 1396. The observations were centered at 5 GHz with 4 GHz of bandwidth and a spectral resolution of 2 MHz. The VLA Configuration was C-array, which has a maximum baseline of 3.4 km and thus an angular resolution of 3.5 arcseconds.

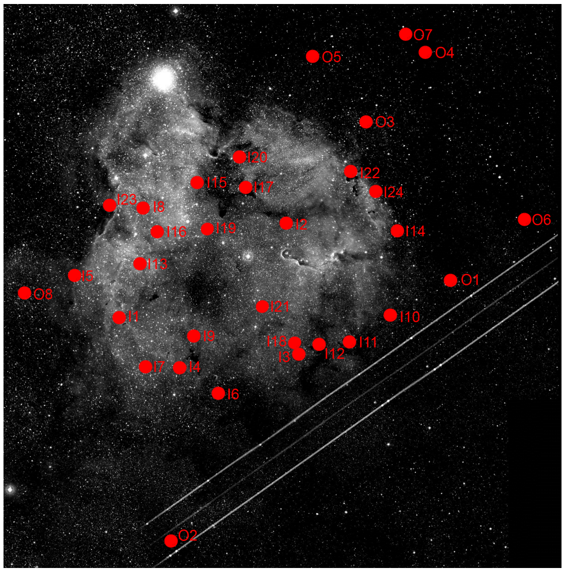

Figure 2: Mosaic of IC 1396 from the Digitized Sky Survey done by the Palomar Observatory. Sources with lines of sight through the region are labelled with 'I', while exterior sources are labeled with 'O'

The sources were selected from the NRAO VLA Sky Survey (NVSS) because they satisfy the criteria of being relatively bright ($> 100\mu$Jy bm^{-1}) and not resolved at 1.42 GHz. The flux density, complex phase, and leakage calibrators are 3C48, J2055+6122, and 3C84, respectively.

The observations had 2 GHz of total frequency coverage, spread across 16 subbands of 128 MHz a piece. The spectral resolution in each subband was 2 MHz, which resulted in 64 frequency bins in each of the subbands. The VLA detects right and left circularly polarized light which give the Stokes parameters of total intensity (I), the linear polarized intensity components (Q and U), and the circular polarized intensity (V).

3. Data Reduction

Data reduction was done through the Common Astronomy Software Applications (CASA) data reduction package. The process of data reduction and calibration is below:

1. We excised data that was corrupted due to radio frequency interference. Often, we removed full antennas as well as data as a function of frequency (e.g., channels or frequency bins). Additionally, we implemented systematic flagging such as "Quack" and "Shadow" flagging, which are standard data reduction techniques.

2. We reduced the data following standard practices. This includes correcting for potential instrumental and external conditions that would impact our observations. These were done by following the CASA *VLA Continuum Tutorial* and included:
   - Antenna position corrections
   - Elevation calibration
   - Initial Flux density scaling
   - Initial Phase calibration
   - Delay calibration
   - Bandpass calibration
   - Gain calibration
   - Polarization calibration

3. Imaging: Using the CASA task TCLEAN, e produced CLEANed maps of Stokes parameters I, Q, U, and V. The restoring beam across all frequency bands was 5.53".

4. We exported the imaged data to FITS files for processing in Python.

4. Data Analysis

4.1 Spectral Index

We calculated the spectral indices, α, of the extragalactic sources to verify whether they generated synchrotron emission. This is a measure of the intensity varying with frequency as described by the power law relationship of $S_\nu \propto \nu^\alpha$. Franzen et al. (2014) report an α range of -1.5 to -0.5 from their study of 85 galaxies, and our measurements are consistent with this range.

We fit for the spectral index using the curvefit function of the Python package, Scipy. Table 1 gives the values of α for each of the sources.

Table 1: Spectral Indices

Source	α
I19	-0.71 $\pm$ 0.14
I20	-0.79 $\pm$ 0.15
I6	-1.11 $\pm$ 0.15
O5	-0.99 $\pm$ 0.15

4.2 Imaging

After examining maps of the Stokes parameters *I, Q, U, V* and confirming that our sources emitted non-thermal radiation, we made maps of the polarization position angle, χ, and the linear polarized intensity, P. These were made for each source and frequency. Two of these maps are shown in Figure 3. We calculated P and χ with Stokes parameters Q and U using the relationships in Equations (3) and (4).

$$P = \sqrt{Q^2 + U^2} \tag{3}$$

$$\chi = \frac{1}{2} \arctan\left(\frac{U}{Q}\right) \tag{4}$$

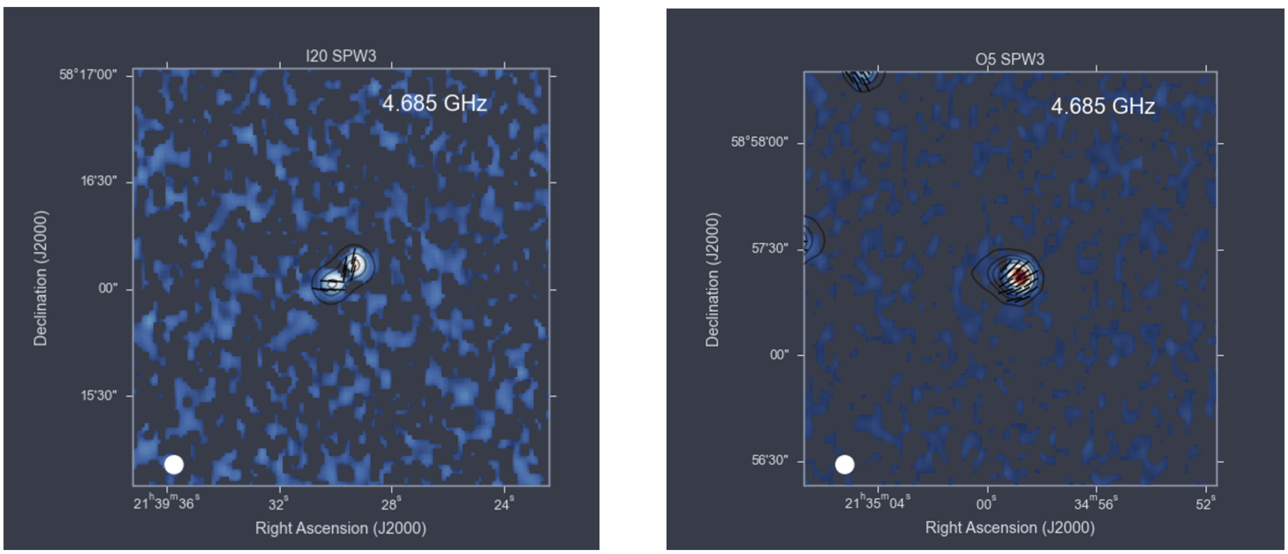

Figure 3: Maps of (left) I20 and (right) O5 at selected frequencies, which are noted in the upper left of each panel. The contours represent the total intensity, I, the vectors represent the polarization position angle, χ. The raster map is the linear polarization intensity, P. The filled white circle in the lower left indicates the restoring beam of 5.53$''$.

4.3 Rotation Measure

Table 2: Calculated Rotation Measures

Source	RM (rad m^{-2})
I19	-605 $\pm$ 29
I20	-202 $\pm$ 42
I6	-248 $\pm$ 16
O5	-140 $\pm$ 6

The Rotation Measure value for each of the sources was calculated using Equation (2) by plotting χ, the polarization position angle, against λ^2. We determined the RM by fitting to the relationship using the curvefit function of the Python package, Scipy. An example of this is show in Figure 4. The RM values for each of the four sources are given in Table 2.

4.4 Plasma Shell Model

We adopt a simple shell model from Savage et al. (2013) to represent the plasma structure of the HII region. In this model, we assume that the HII region is comprised of a low density inner cavity as a result of a ionization front that has propagated outward from the central star. We call this the inner radius of the shell, R_I. This cavity has less dense photoionized material. Between this and the outer radius of the shell, R_O, there is a region of denser photoionized material. Past R_O, we assume a constant n_e value. The following equation models a simplified structure of the region and the expected RM in the shell,

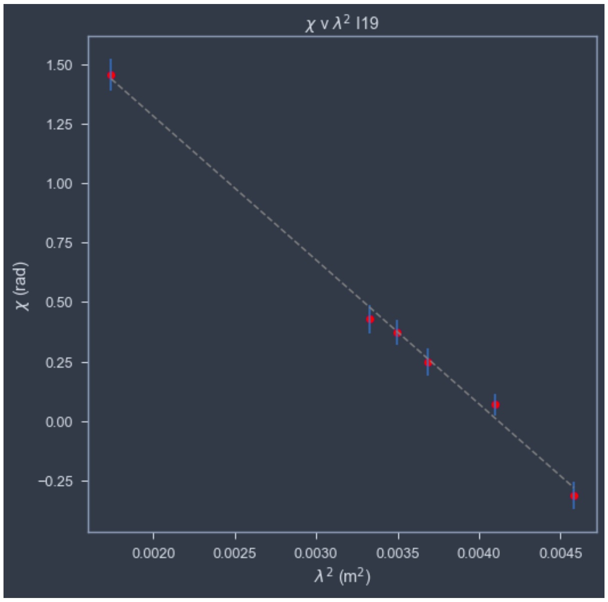

Figure 4: Plot of the χ in radians against λ^2 in m^2 for I19. The best-fit RM value is -605 $\pm$ 29 rad m^{-2}.

$$RM(\xi_{src}) = 0.81\ n_e\ L(\xi_{src})\ B_{\|} \tag{5}$$

where L(ξ) is the effective thickness of the HII region along a line of sight and ξ represents the linear distance between the line of sight passing though the center of the shell and the the line of sight passing through the outer edge of the shell. I adopt as a geometric center for the nebula the position of the exciting star cluster HD 206267A. The electron density, n_e, is in units of cm^{-3}, $B_{\|}$ is in units of μG, and L(ξ) is in units of parsecs (pc).

We modeled $L(\xi)$, the chord length through the shell, using the following equations,

$$L(\xi) = 2R_I \sqrt{\left(1 - \left(\frac{\xi}{R_I}\right)^2\right)} \text{ if } \xi \geq R_O \tag{6}$$

$$\begin{aligned} L(\xi) = 2R_I \Bigg[& \sqrt{\left(1 - \left(\frac{\xi}{R_I}\right)^2\right)} \\ & - \left(\frac{R_O}{R_I}\right) \sqrt{\left(1 - \left(\frac{\xi}{R_O}\right)^2\right)} \Bigg] \quad \text{if } \xi \leq R_O \end{aligned} \tag{7}$$

To describe the RM as a function of distance from the star cluster, we need to determine the shell parameters of R$_I$ and R$_O$ and measure the electron density. We utilized the Canadian Galactic Plane survey radio image at 1.42 GHz of IC 1396. We measured T_B, the brightness temperature (which is a measure of the intensity of electromagnetic energy in units of K) as a function of ξ along slices taken through the nebula, and fit the extracted data with Equations 6 and 7. We took radial slice in the plane of the sky and they intersected the lines of sight to the extragalactic sources. This translated to extracting lines of pixels from the central star cluster out to the edge of the image. Each pixel contained brightness temperature data. We stored the distances from the central star cluster to each pixel along the line as well as the associated brightness temperatures.

The extragalactic sources are significantly brighter than the diffuse emission of the nebula. To disentagle the two, we masked the contribution of the emission from the extragalatic source. The emission contributions manifested as large spikes in brightness temperature in the plots. We fit a homogeneous spherical shell model to each radial slice of thermal emission passing through each source (shown in Figure 6), allowing me to calculate the electron density described in the steps below:

- We specified ξ to be the exact distance to the extragalactic source and extracted the brightness temperature, T_B, at ξ from the best-fit model of $T_B(\xi)$.
- We calculated the chord length $L(\xi)$ in pc using the parameters of the shell model, R_I and R_O, as well as the source ξ, using Equation 6.
- Thereafter, we solved for the emission measure (EM) in Equation 8 using the model brightness temperature T_B at the distance to

the source.

$$\text{EM} = 282\ T_8^{0.35}\ \nu_{\text{GHz}}^{2.1} T_B(\xi_{src})\ \text{cm}^{-6}\ \text{pc} \tag{8}$$

where T_8 is in units of 8000 K and is the electron temperature, ν_{GHz} is the frequency T_B is measure at, which is 1.42 GHz in this case.

- We took $L(\xi)$ obtained from 6 and the calculated EM from Equation 8 and substitute these into Equation 9 solving for n_e. f is a filling factor of 1. The filling factor accounts for how dense the material in the region is and we assume it is uniformly filled, with a constant electron density along a line of sight.

$$\text{EM} = \int n_e^2\, dz = f n_e^2\, L(\xi_{src}) \tag{9}$$

- Finally, for sources that we had measured RM values of (see Table 2), we solved for $B_{||}$ using Equation 5.

Table 3 gives the calculated parameters of R_I, R_O, n_e, $L(\xi)$ for all 28 sources, as well as 4 calculated RM values. We calculated parallel component of the vector magnetic field for 2 out of the four sources, I19 and I20; these being -2.4 μG and -0.5 μG respectively. A cartoon depicting the shell model and how the parameters, measured brightness temperature and slices manifest is shown in Figure 5.

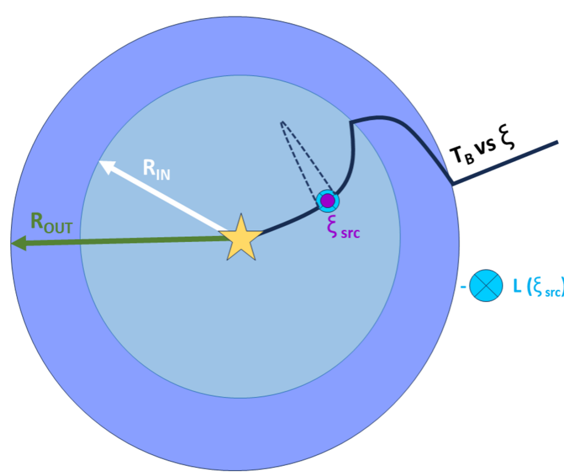

Figure 5: Cartoon depicting the shell model of plasma region, defining several variables discussed earlier in Section 4.4

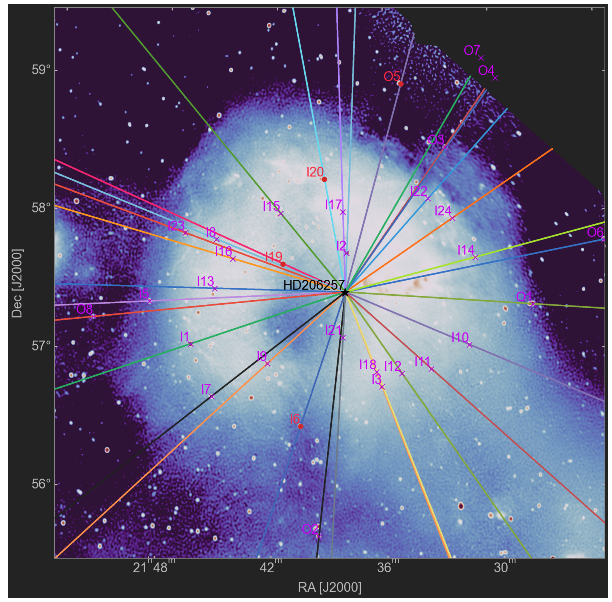

Figure 6: Mosaic of a radio image of IC 1396 taken at 1.42 GHz by the Canadian Galactic Plane survey depicting the 31 slices taken radially from a line of sight at the central star cluster to the line of sight of the extragalactic sources.

To model the brightness temperature as a function of ξ, we implemented a number of methods and assessed their effectiveness. Using Equations 6 and 7, we first fit the raw data using the curvefit function of the Python package, Scipy. These fits were skewed by the spikes corresponding to emission from the extragalactic sources, as well as other potential background galaxies separate from our 31 sources. We then masked the extragalactic sources by eye and applied my fitting code, which resulted in much closer fitted plots. As we did this by eye, there is a level of subjectivity that cannot be accounted for quantitatively in the analysis. For plots corresponding to source including I6, O2, I1, I5, I21, I16, I13, I9, I8, I7, and O8, we excised data that appeared to have peaks of emission from near the center of the shell as these caused to return erroneous parameters. We attribute the inflation in the emission to foreground or background shell emission along the line of sight.

As the data could often be noisy, we applied a kernel smoothing function known as the Savitzky–Golay filter through Python's Scipy package to increase the precision of the data fits. This smoothing function had a parameter known as window_length that we could change to adjust the size of the data point subsets used for the smoothing process. We used an average of 85 for this parameter across the 31 T_B vs. ξ plots. We smoothed the raw data and fitted to it, and found that by not masking the emission spikes, the curve did not fit well to the data.

Finally, we investigate how the results changed when both applications were applied. We masked the data by eye and then applied the Savitzky–Golay filter prior to fitting the data. This yielded well-fitted curves that were often identical to the non-smoothed masked fits. For parameter results, we decided to use the results of the smoothed-masked fits as for noisier data, the curve-fit was more effective. For examples of all 4 fitting processes, refer to Figure 7.

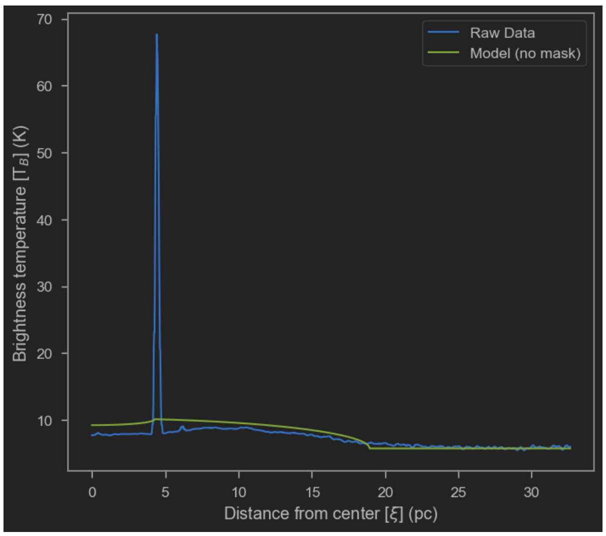

(a)

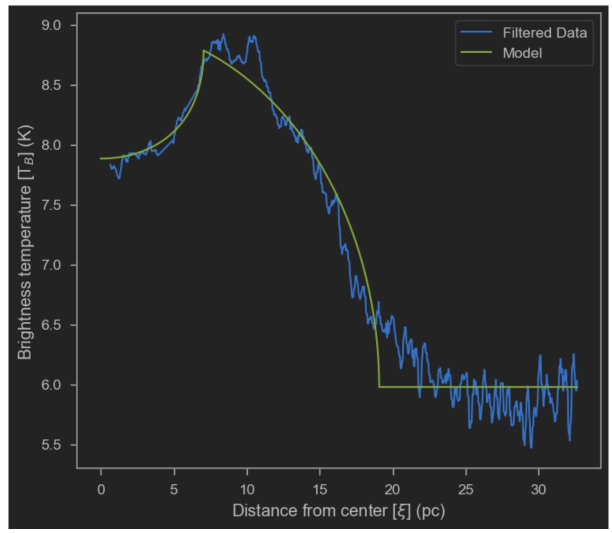

(b)

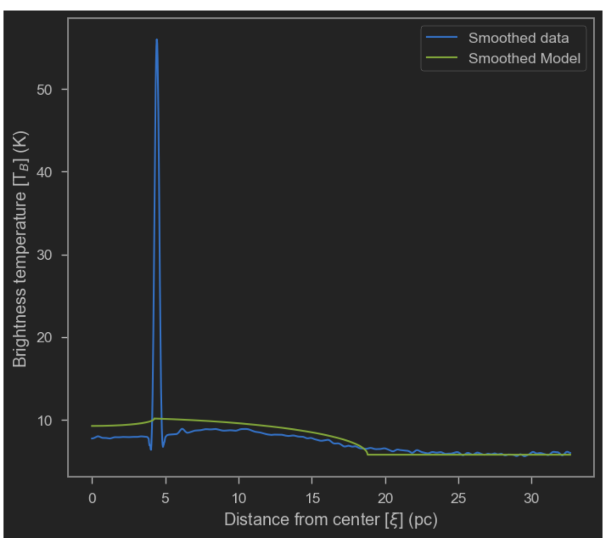

(c)

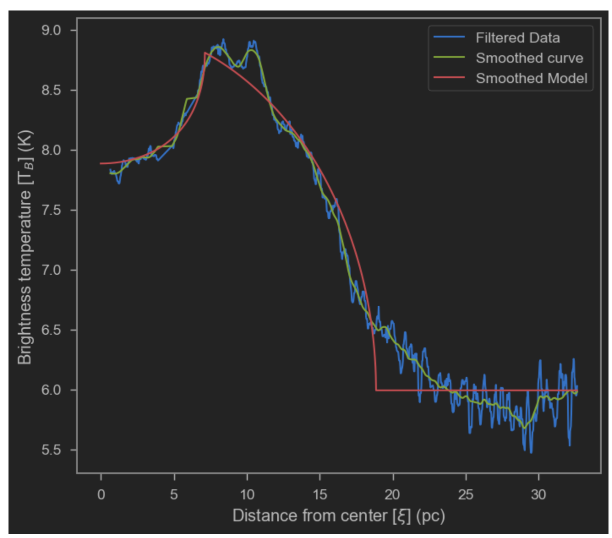

(d)

Figure 7: Plots of the measured brightness temperature from the 1.42 GHz radio continuum map as a function of ξ (pc) from the center of IC 1396 to the source I2 depicting 4 fitting methods. (a) Fit applied to raw data, (b) Fit applied to data where emission contribution from I2 has been excised (Filtered Data), (c) Fit applied to data smoothed by Savitzky–Golay filter, (d) Fit applied to data masked and then smoothed by Savitzky–Golay filter.

Table 3: Parameters resulting from Plasma shell model. Sources that had undetermined chord lengths and electron densities (due to failing the fitting domains) were left blank.

Name	$R_O(pc)$	$R_I(pc)$	L(ξ) (pc)	RM (rad m^{-2})	n_e (cm^{-3})
O6	20.9	4.0			
O1	20.1	3.9			
O3	15.5	6.5			
O5	17.1	6.0		-140 $\pm$ 6	
I3	18.1	4.5	19.3		15.1
I2	18.5	7.1	23.7		14.1
O2	16.4	6.3			
I6	15.6	6.5		-248 $\pm$ 17	
I1	23.5	13.3	31.7		11.9
I23	21.5	11.5	28.7		12.8
I5	22.0	11.7	18.1		15.4
I24	18.6	4.9	18.2		15.5
I22	16.5	5.3	15.3		17.0
I21	17.3	6.6	30.3		12.3
I20	21.1	7.7	37.1	-202 $\pm$ 42	11.6
I19	21.6	10.5	22.9	-605 $\pm$ 29	13.9
I18	17.4	4.5	21.6		14.4
I17	19.7	7.2	32.8		12.3
I16	21.2	11.6	25.8		13.4
I15	24.3	7.6	46.0		10.2
I14	19.1	4.8	13.7		17.2
I13	21.7	11.5	35.8		11.7
I12	16.6	5.0	12.5		18.6
I11	16.2	4.3			
I10	22.1	3.7	21.8		14.0
I9	24.7	13.6	32.3		11.5
I8	21.5	11.0	35.2		11.8
I7	25.7	12.6	33.8		11.2
O4	15.5	6.2			
O7	16.3	6.2			
O8	22.2	12.0			

5. Discussion

We report results for four extragalactic sources: I19, I20, I6, and O5. The first three sources had lines of sight through IC 1396, while O5 had a line of sight external to the region. As detailed in Section 6.1, we calculated the spectral indices of these sources and they were all consistent with non-thermal synchrotron sources. The range of RM values we found for these sources was from -605 to -140 rad m^{-2}. As a consistency check, we compared the observed RM values with a rough estimate of the RM due to a galactic HII region using typical values for electron density of 10 cm^{-3} and a magnitude of the Galactic magnetic field B_0 assumed to be 6 μG. $B_{\|}$ is the parallel component of the magnetic field of the HII region, θ is the angle between the line of sight and an azimuthal magnetic field, which for a Galactic longitude of 99.3° for IC 1396 is calculated to be 23°.

$$RM_{exp} \propto n_e B_{\parallel} L \text{ where } B_{\parallel} = B_0 \cos(\theta) \quad (10)$$

Using these assumptions, the expected |RM| value of the HII region was ~525 rad m^{-2}.

Additionally, we compared our results to the predicted Galactic RM values presented in Van Eck et al. (2011). Their model assumes the Galactic magnetic field follows the spiral arm structure. The area of the galaxy in which IC 1396 lies has predicted RM values ranging from -200 to -50 rad m^{-2}. We concluded from this comparison that the RM value for the exterior source O5 is consistent with this galactic background RM, with no influence from IC 1396. Additionally, the interior sources I19, I20, and I6 are consistent in polarity with the galactic background RM.

Despite I19, I20, and I6 all having lines of sight through the HII region, their RM values varied significantly. I19 had an |RM| value that was in general agreement with the expected value that we calculated. However, I20 and I19 had a RM difference of nearly 403 rad m^{-2} despite having a line of sight through the photoionized gas. I6 had a RM value that was similar to I20. The interior sources do, notably, have an excess RM of 62-465 rad m^{-2} with respect to O5 (i.e., the background RM value). Figure 8 is a radio image depicting the spatial distribution of the 4 extragalactic sources with the RM values scaled relative to each other to show the magnitudes of the RM values.

We have also determined the electron density, within the integrand of Equation (1), along the lines of sight in order to analyze these sources further and to extract information about the magnetic field. To do this, we have followed a similar treatment as described in Costa and Spangler (2018). Additionally, our sources I19 and I20 had two components and the RM value from each source was only partially resolved. Having the RM of the second component of both of these sources would give us a better understanding of how the magnetic field is behaving on smaller scales. Furthermore, for future work, there are several more frequency information to integrate into this analysis, as well as 28 more extragalactic sources that we can analyze. Once we have obtained their RM values, we will be able to conduct a similar extraction of the magnetic field detailed in Section 4.4. Furthermore, we will calculate the RM values using a second method known as Rotation Measure Synthesis, which accounts for the shortcomings of the previous χ^2 method we implemented.

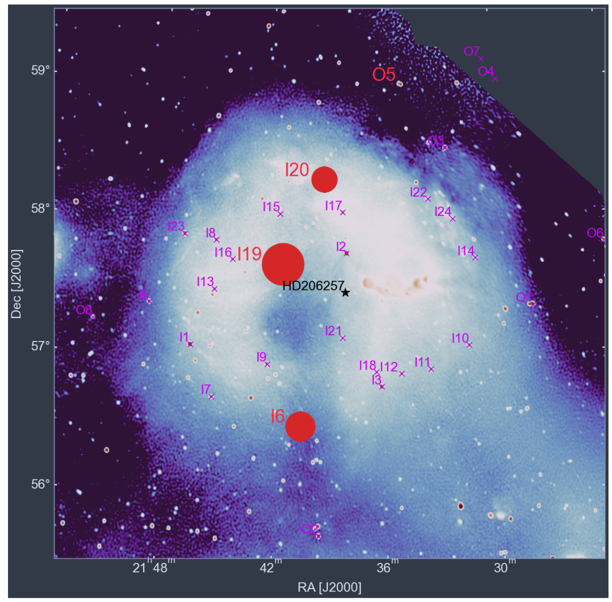

Figure 8: Mosaic of a radio image of IC 1396 taken at 1.42 GHz by the Canadian Galactic Plane Survey. The RM values are scaled relative to each other by subtracting the RM value of O5 from each of the 4 sources. The points in magenta mark the 28 other extragalactic sources. All of the RM values were negative.

6. Summary and Conclusions

- We have VLA polarimetric data for 31 extragalactic radio sources with lines of sight passing through and or near to IC 1396. Here, we report Faraday Rotation measurements for 4 of these sources.
- We calculated the spectral index of each source and confirmed that they emitted nonthermal synchrotron radiation.
- We performed data reduction through the CASA software and created images of Stokes parameters I, Q, U, and V.
- We compared our RM results to an estimate of the RM in the HII region as well as to a predicted Galactic background RM described

by Van Eck et al., 2011 in order to perform a check on our data analysis. we found that only I19 reasonably agrees with the estimate and O5 is consistent with the background RM value in this region of the galaxy. Additionally, we determined that the interior sources with lines of sight through the region have a RM value difference of 62-465 rad m^{-2} with respect to the background RM estimate.

- We implemented a model of the structure of IC 1396 and assessed the electron densities associated with many sources, as well as used brightness temperature profiles from the Canadian Galactic Plane survey image to estimate the thickness of the nebula along a line of sight through a source.

Acknowledgments

R.R. was supported in part by the VSGC Undergraduate STEM Research Scholarship. Additionally R.R. and A.C. would like to thank NRAO, which is a facility of the National Science Foundation, operated under cooperative agreement with Associated Universities, Inc.

References

Chlebowski, T. and Garmany, C. D. (1991). On Winds and X-Rays of O-Type Stars. *The Astrophysical Journal*, 368:241.

Costa, A. H. and Spangler, S. R. (2018). A Faraday Rotation Study of the Stellar Bubble and H II Region Associated with the W4 Complex. *The Astrophysical Journal*, 865(1):65.

Costa, A. H., Spangler, S. R., Sink, J. R., Brown, S., and Mao, S. A. (2016). Denser Sampling of the Rosette Nebula with Faraday Rotation Measurements: Improved Estimates of Magnetic Fields in H II Regions. *The Astrophysical Journal*, 821(2):92.

Franzen, T. M. O., Sadler, E. M., Chhetri, R., Ekers, R. D., Mahony, E. K., Murphy, T., Norris, R. P., Waldram, E. M., and Whittam, I. H. (2014). Deep 20-GHz survey of the Chandra Deep Field South and SDSS Stripe 82: source catalogue and spectral properties. *The Monthly Notices of the Royal Astronomy Society*, 439(2):1212–1230.

Savage, A. H., Spangler, S. R., and Fischer, P. D. (2013). Probing the Rosette Nebula Stellar Bubble with Faraday Rotation. *The Astrophysical Journal*, 765(1):42.

Strömgren, B. (1939). The Physical State of Interstellar Hydrogen. *The Astrophysical Journal*, 89:526.

Tarricq, Y., Soubiran, C., Casamiquela, L., Cantat-Gaudin, T., Chemin, L., Anders, F., Antoja, T., Romero-Gómez, M., Figueras, F., Jordi, C., Bragaglia, A., Balaguer-Núñez, L., Carrera, R., Castro-Ginard, A., Moitinho, A., Ramos, P., and Bossini, D. (2021). 3D kinematics and age distribution of the open cluster population. , 647:A19.

Van Eck, C. L., Brown, J. C., Stil, J. M., Rae, K., Mao, S. A., Gaensler, B. M., Shukurov, A., Taylor, A. R., Haverkorn, M., Kronberg, P. P., and McClure-Griffiths, N. M. (2011). Modeling the Magnetic Field in the Galactic Disk Using New Rotation Measure Observations from the Very Large Array. *The Astrophysical Journal*, 728(2):97.

Whiting, C. A., Spangler, S. R., Ingleby, L. D., and Haffner, L. M. (2009). Confirmation of a Faraday Rotation Measure Anomaly in Cygnus. *The Astrophysical Journal*, 694(2):1452–1463.